

# COMPARISON OF CELL MECHANICAL MEASUREMENTS PROVIDED BY ATOMIC FORCE MICROSCOPY (AFM) AND MICROPIPETTE ASPIRATION (MPA)

Rafael Daza<sup>1,2</sup>, Blanca González-Bermúdez<sup>1,2</sup>, Julia Cruces<sup>4</sup>, Mónica De la Fuente<sup>4</sup>, Gustavo R. Plaza<sup>1,2</sup>, María Arroyo-Hernández<sup>1,3</sup>, Manuel Elices<sup>1,2</sup>, José Pérez-Rigueiro<sup>1,2,5</sup>, Gustavo V. Guinea<sup>1,2,5</sup>

1. Centro de Tecnología Biomédica. Universidad Politécnica de Madrid. 28223 Pozuelo de Alarcón (Madrid). Spain

2. Departamento de Ciencia de Materiales. ETSI Caminos, Canales y Puertos. Universidad Politécnica de Madrid. 28040. Madrid. Spain

3. Departamento de Biotecnología. Faculty of Experimental Sciences. Francisco de Vitoria University (UFV). 28223. Pozuelo de Alarcón (Madrid). Spain

4. Departamento de Fisiología Animal II. Facultad de Biología. Universidad Complutense de Madrid. 28040. Madrid. Spain

5. CIBER-BBN, Biomedical Research Networking Center in Bioengineering Biomaterials and Nanomedicine, Spain

## Abstract

A comparative analysis of T-lymphocyte mechanical data obtained from Micropipette Aspiration (MPA) and Atomic Force Microscopy (AFM) is presented. Results obtained by fitting the experimental data to simple Hertz and Theret models led to non-Gaussian distributions and significantly different values of the elastic moduli obtained by both techniques. The use of more refined models, taking into account the finite size of cells (simplified double contact and Zhou models) reduces the differences in the values calculated for the elastic moduli. Several possible sources for the discrepancy between the

techniques are considered. The analysis suggests that the local nature of AFM measurements compared with the more general character of MPA measurements probably contributed to the differences observed.

Keywords: mechanobiology, T cell, elastic modulus, classical models, finite size effect.

## Introduction

Mechanical characterization of cell behavior is a relatively new scientific discipline which addresses the analysis of mechanical properties of cells and their relation with the mechanobiological processes that take place during the cell life cycle (growth, motility or cell division, among others) (Ingber. 2003, Jansen et al. 2015, Wang and Thampatty. 2006). The relevance of mechanical properties at cell level justifies the development of different experimental techniques in order to characterize them and the creation of different mechanical models to interpret the data measured by these techniques (Lim et al. 2006). Among them, micropipette aspiration (MPA) and atomic force microscopy (AFM) are two commonly used techniques.

Micropipette aspiration, developed by Mitchison and Swann (Mitchison and Swann. 1954), uses a microcapillary with a smaller inner diameter than the cell diameter. When suction pressure is applied, the cell undergoes a deformation process while being inserted in the microcapillary. By measuring the geometry of the cell inside the capillary as a function of suction pressure, it is possible to assess the cell mechanical behavior, although a mechanical model is required to interpret the experimental data. Initial models (Theret et al. 1988) considered the cell as an elastic semi-infinite space. In subsequent refinements, cells were modeled as elastic spheres (Zhou et al. 2005, Esteban-Manzanares et al. 2017).

The aforementioned AFM allows some mechanical properties of cells based on a different physical principle to be measured (Binnig et al. 1986). AFM probes the cell surface by means of a cantilever with a sharp tip at one end. The cantilever tip indents the cell and a force-displacement curve is obtained. Data interpretation requires a mechanical model for the tip-cell contact. As a first approach, Hertz's single contact mechanical model (Hertz. 1882, Hertz. 1896), which considers the sample as an elastic semi-infinite space, is routinely used. More sophisticated models have been developed to take into account the finite size of samples (Dimitriadis et al. 2002, Vichare et al. 2012). In particular, the simplified double contact model (SDC) proposed by Glaubitz et al. (Glaubitz et al. 2014) has been shown to be a necessary refinement when the sample has a

finite size and a spherical shape. The SDC model considers both the contact between the AFM tip and the cell, and between the cell and the substrate.

MPA and AFM have been extensively used to characterize the mechanical behavior of different cell lineages such as erythrocytes (Rand and Burton. 1964, Jiao et al. 2009, Dulińska et al. 2006), neutrophils (Roca-Cusachs et al. 2006, Derganc et al. 2000), chondrocytes (Allen and Mao. 2004, Florea et al. 2014, Guilak et al. 2006) or lymphocytes (Daza et al. 2015, Schmidtschonbein et al. 1981, Schneider et al. 1987, Rosenbluth et al. 2006). However, although both techniques were developed to characterize cell mechanical behavior, significant differences in the underlying deformational mechanisms cast doubts on the equivalence of numerical results obtained by both techniques. The clearest difference between AFM and MPA is related to the direction along which forces are applied, and the directly affected volume fraction. Additionally, cells must remain sufficiently adhered to the substrate and any lateral movement of the cell must be avoided during the AFM indentation process. Cell immobilization could influence mechanical response and, at the very least, this boundary condition should be taken into account when applying the theoretical models. In contrast, cells must be completely detached during characterization by MPA. Ideally, these differences in the physical principles of both experimental techniques should not represent an obstacle to accurately determining cell mechanical behavior, as they should be taken into account when modeling the experimental data. In practice, however, when Bader et al. (Bader et al. 2002) analyzed the mechanical properties of chondrocytes by means of MPA and AFM, the discrepancy in the elastic moduli obtained from both techniques led the authors to the conclusion that it is not possible to define the mechanical behavior of the cells with only one parameter. Dahl et al. (Dahl et al. 2005) found a similar discrepancy when using MPA and AFM to probe the viscoelastic behavior of isolated cellular nuclei. Differences in the spatial distribution of applied forces were identified as the basic origin of this discrepancy. The importance of the different spatial distribution of applied forces was also highlighted by Darling et al. (Darling et al. 2006)

Since elasticity represents a biophysical property closely related to physiological and/or pathological processes of the cell and their interaction with their

surrounding environment (Schillers et al. 2017), it would be desirable to establish a relationship that could compare the values provided by MPA and AFM, when used to characterize the mechanical behavior of the cells.

As mentioned above, discrepancies in the values of the mechanical parameters provided by AFM and MPA are usually attributed to the different experimental procedures of both techniques. In this regard, the possible effects of the mechanical models required to deduce the data are assigned a secondary role. This paper analyzes the influence of using different models to fit the data obtained from MPA and AFM in an attempt to reduce the discrepancies in the mechanical parameters obtained from both techniques. Accordingly, the elastic behavior of non-adherent T cells was measured by MPA and AFM and the results were compared. The experimental data obtained from both techniques were fitted to the classical Theret's and Hertz's models and, additionally, to the more refined models proposed by Zhou and Glaubitz, which take into account the finite size of the samples. Data analysis showed a non-Gaussian distribution for the calculated elastic moduli; therefore, other statistical distributions were tested. The Gamma distribution function is shown to fit the experimental results and allows the corresponding mechanical parameters to be determined. Comparison of the data obtained from MPA and AFM shows relatively significant differences even if the refined models are used. The local nature of AFM measurements in contrast to the global character of MPA measurements might be partly responsible for the differences observed.

## Materials and methods

### *Acquisition and preparation of cells*

Female ICR-CD1 mice (*Mus musculus*) were used, after being obtained from Janvier S.A.S. (Le Genest-St-Isle, France) at the age of seven to eight months. They were specific-pathogen-free, according to Federation of European Laboratory Science Associations (FELASA) recommendations. The mice were randomly allocated in groups of five individuals per cage (50 x 25 cm polyurethane boxes), at a constant temperature ( $22 \pm 2$  °C) in sterile conditions, inside an aseptic air negative-pressure environmental cabinet (Flufrance,

Cachan, France), on a 12/12 h reversed light/dark cycle (lights were switched on at 8:00 h and off at 20:00 h). The mice had access to tap water and standard Sander Mus pellets (the A04 diet from Panlab L.S. Barcelona) *ad libitum*. This diet was in accordance with the recommendations of the American Institute of Nutrition for laboratory animals. The mice were marked for individual follow-up. The experimental protocol was approved by the Animal Ethics Committee of the Universidad Complutense de Madrid. The animals were treated according to the guidelines of the *European Community Council Directives 1201/2005 EEC*.

Peritoneal leukocytes were obtained from the mice, between 8:00h and 10:00 h, without killing the animals. Each mouse was held by its cervical skin and its abdomen cleansed with 70% ethanol. Subsequently, 3ml of sterile Hank's solution (Sigma-Aldrich, Tres Cantos, Spain), previously tempered at 37°C, was injected intraperitoneally. After massaging the abdomen, 80% of the injected volume was recovered. Peritoneal leukocytes were counted in Neubauer chambers (Blau Brand, Germany). Cellular viability was routinely checked by the Trypan Blue (Sigma, St Louis, MO) exclusion test, and only suspensions with cell viability higher than  $99 \pm 1$  % were used. The cells were maintained at 4°C throughout the implementation of experimental protocols.

In order to isolate non-adherent lymphocytes from the peritoneal leukocyte population, the suspension obtained from each mouse was incubated at 37°C in a humidified atmosphere of 5% CO<sub>2</sub>, for 45 minutes, by using migratory inhibitory factor plates (Kartell, Noviglio, Italy). After this time, the supernatants, mainly consisting of non-adherent lymphocytes, were collected by using a Pasteur pipette. Lymphocytes were identified by their morphology and quantified in Neubauer chambers through the use of optical microscopy (x40). Additionally, the purity of lymphocyte suspension was confirmed by immunostaining with monoclonal antibodies for the expression of CD45, CD3 and CD19 (BD Pharmingen, San Diego, CA), conjugated with different fluorochromes. Fluorescence was measured by using a flow cytometer (FACSCalibur; Becton Dickinson, Franklin Lakes, NJ). The results were analyzed with Cell Quest Pro software (BD Biosciences, San Jose, CA). The

percentage of T lymphocytes obtained after the isolation protocol used for the subsequent experiments was higher than 86%.

### *AFM measurements*

The baseline lymphocyte concentration was set at  $2.5 \cdot 10^5$  cell/ml. All samples were subjected to vortex stirring in order to ensure homogeneous cell distribution. A volume of 100  $\mu$ l was deposited on an activated vapor silanization (AVS) functionalized silicon surface (Arroyo-Hernandez et al. 2014) used as substrate for AFM observation. The cells were incubated on the substrates for two hours at nominal conditions of 25°C and 40% relative humidity. Cells not attached to the surface were removed by rinsing them with filtered Hank's solution.

Cell indentation tests were carried out by following the same procedure used to characterize the mechanical properties of T lymphocytes presented in a previous published work (Daza et al. 2015). Briefly, an initial approach movement based on hydrodynamic forces was used in order to bring the tip into proximity with the cells (the procedure followed asserted that the distance between tip and substrate is always higher than 10  $\mu$ m). Next, 100 x 100  $\mu$ m<sup>2</sup> areas were scanned by the tip with the AFM operating in jumping mode (de Pablo et al. 1998, Moreno-Herrero et al. 2004) until a cell was detected. The scan was then stopped and deflection-displacement curves were recorded. More than 30 curves were obtained for each cell. Each curve consisted of 512 sampling points and all were obtained at a constant loading rate of 1  $\mu$ m s<sup>-1</sup>. A Cervantes AFM (Nanotec Electrónica S. L., Madrid) was used for imaging and for the mechanical characterization of lymphocytes. This entailed using relatively soft cantilevers (Olympus OMCL-RC800) with spring constants  $k_c = 0.05$  Nm<sup>-1</sup> as determined by the Sader method (Sader et al. 1999), a half-cone angle of  $\theta = 35^\circ$  (measured in our laboratory from SEM images, FESEM Auriga Zeiss) and tip radius of 15 nm (measured in our laboratory from SEM images, FESEM Auriga Zeiss) (Figure S1).

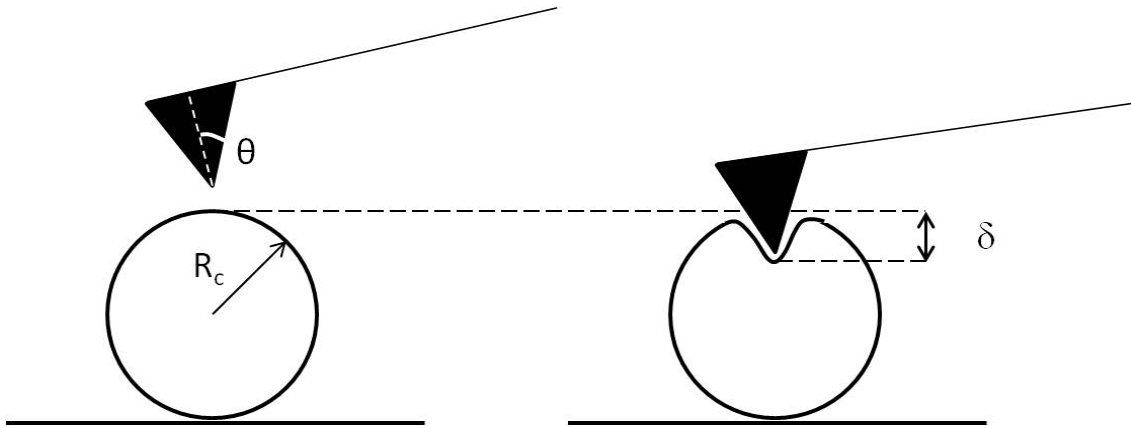


Figure 1. Diagram with the main geometrical parameters used to estimate the elastic modulus of the lymphocytes with AFM before (left) and after (right) the cell being indented.

Cantilever deflection - sample displacement curves were transformed into force-displacement curves and fitted both to the classical Hertz's model and the SDC model. Both models relate the applied force with the induced deformation  $\delta$  (Figure 1). Since the SDC model is applied to finite samples, it was necessary to measure cell size by using AFM images of each indented T-lymphocyte. Cell radius was obtained as a function of the height ( $h$ ) and the secant length ( $x$ ), as shown in Figure 2. Since the distance between tip and substrate is higher than the maximum  $z$  piezoscaner displacement, it should be clarified that  $h$  does not show real cell height but only the size of the small dome probed. AFM cell imaging experiments were performed in a liquid environment in jumping mode with a normal force set-point value of 0.2 nN. Processing the AFM images consisted of equalizing and adjusting contrast and brightness of the micrographs with the software WSxM (Nanotec Electrónica, Spain) (Horcas et al. 2007). Determination of cell size was obtained from AFM images of the cell surface (Figure 2), assuming a spherical shape.

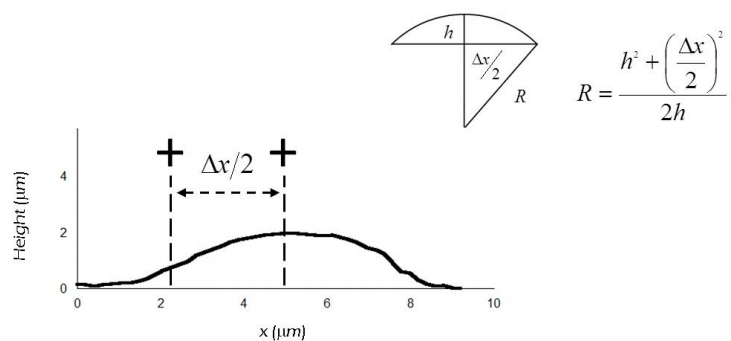
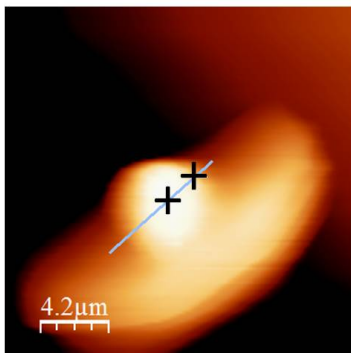




Figure 2. AFM topographical image of a T lymphocyte (the “halo” around the cell is an artifact which was attributed to a mechanical contact between cell and cantilever (Daza et al. 2015)). The blue line shows the path with a profile shown in the right -hand image. The black crosses indicate the position in which the cell dimensions were measured.

### *Micropipette aspiration tests*

Micropipette-aspiration experiments were conducted by using the custom-built device described above (Plaza et al. 2014, Esteban-Manzanares et al. 2017), using microcapillaries with a nominal internal diameter of 5  $\mu\text{m}$ . The cell suspension (0.5 ml) was deposited on a cover-glass plate placed in an optical Meiji TC5400 inverted microscope. The microcapillary was connected to a distilled water reservoir and differential pressure was applied by varying the height of the reservoir. This differential pressure  $\Delta P$  was applied at a constant rate of 0.5 Pa/s as described in Esteban-Manzanares et al. (Esteban-Manzanares et al. 2017). The images were analyzed with the software IMAGEJ (see: <http://rsb.info.nih.gov/ij>), and the length  $L$  of the cellular material inside the microcapillary, the outside radius  $R_c$  and the pipette radius  $R_p$  were measured (Figure 3).

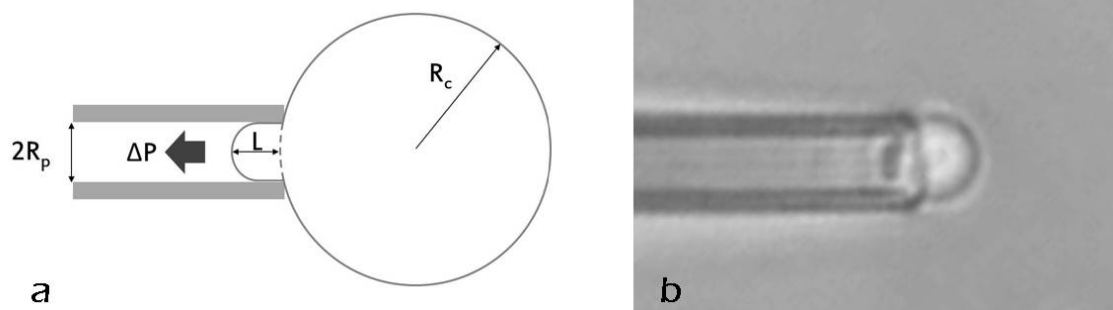


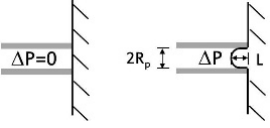
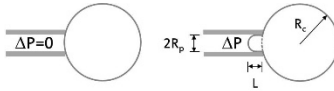
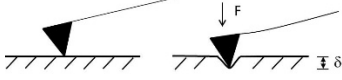
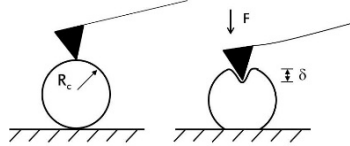
Figure 3. (a) Scheme of the main dimensions used to estimate the elastic modulus of the T lymphocyte with MPA, (b) optical microscope image of the micropipette and the deformed T cell.

### *Mechanical models*

The experimental data were analyzed by means of two sets of mechanical models: those which consider the cell as an infinite half space and those which take into account the finite size of the cells. In particular, MPA data were interpreted following the models proposed by Theret et al. (Theret et al. 1988)

(who hypothesized the cell as an infinite half space) and Zhou et al. (Zhou et al. 2005) (where the cell is considered as a finite body). AFM data were fitted to Hertz's contact model (Hertz. 1896, Hertz. 1882) (which considers a semi-infinite sample) and the simplified double contact model (SDC) deduced by Glaubitz et al. (Glaubitz et al. 2014). Table 1 summarizes the expressions used to estimate the elastic modulus of the T-cells from the experimental data with each model. All the analyses were made by considering the cells as an incompressible material (Costa. 2006), which implies assigning a value of 0.5 to the Poisson's coefficient ( $\nu$ ) in Table 1.

**TABLE 1. Models used to analyze MPA and AFM mechanical data<sup>1</sup>**

	Infinite half-space	Finite size
	Theret et al. 1988	Zhou et al. 2005
MPA	$\frac{L}{R_p} = \frac{3 \Delta P}{2\pi E} \Phi_p$ 	$\frac{3 \Delta P}{E} = \left[ \beta_1 \frac{L}{R_p} + \beta_2 \left( \frac{L}{R_p} \right)^2 \right] \left[ 1 - \left( \frac{R_p}{R_c} \right)^{\beta_3 + \beta_4 \frac{L}{R_p} + \beta_5 \left( \frac{L}{R_p} \right)^2} \right]$ $\beta_1 = 2.0142, \beta_2 = 2.1186, \beta_3 = 2.1187, \beta_4 = -1.4409$ 
	Hertz. 1896, Hertz. 1882	Glaubitz et al. 2014
AFM	$\delta = \left( \frac{\sqrt{2} F (1 - \nu^2)}{E \tan \theta} \right)^{1/2}$ 	$\delta = \left( \frac{\sqrt{2} F (1 - \nu^2)}{E \tan \theta} \right)^{1/2} + \left( \frac{3 F (1 - \nu^2)}{4 E R_c^{1/2}} \right)^{2/3}$ 

<sup>1</sup> The parameters shown in each expression stand for the following parameters:  $R_c$ ,  $E$  and  $\nu$  are, respectively, the radius, the elastic modulus and Poisson's ratio of the cell;  $L$  is the length of cell inside a micropipette of radius  $R_p$  when a suction pressure of  $\Delta P$  is applied,  $\Phi_p$  is a pipette geometric factor which is typically taken as  $\approx 2.1$ ;  $\delta$  represents the indentation depth achieved when a pyramidal cantilever with semi-angle  $\theta$  applies a force  $F$ .

### *Confocal images*

T Lymphocytes were placed on a functionalized silicon surface for two hours. After this time, cells not attached to the surface were removed by rinsing with filtered Hank's solution and, finally, this solution was replaced with PBS. Each sample was subsequently put in a well with 400  $\mu$ L of 0.1% Triton solution and mechanically shaken for 30 minutes. Subsequently, Triton solution was replaced with a phalloidin-rhodamine solution (1:1000 in PBS) which remained in contact with the sample for a term of 30 minutes. 25 minutes after combing this solution with the lymphocytes, a DAPI solution (1:5000 in PBS) was added. Finally, this solution was replaced with Mili-Q water after a series of rinses with filtered PBS. Each sample was labeled and appropriately packed. The day prior to observation, samples were stained with a fluorescent solution (Mowiol with p-phenylenediamine 0.1%). Confocal images of more than ten T-lymphocytes were obtained by means of Olympus FV1200 confocal microscope.

### *Statistical analysis*

The statistical software Statgraphics Centurion was used for performing statistical analysis of the experimental data collected from both techniques. In particular, Kolmogorov-Smirnov (Massey. 1951, Öztuna et al. 2006) and Shapiro-Wilk (Shapiro and Wilk. 1965, Shapiro and Francia. 1972) tests were carried out in order to assess normality. The Kolmogorov-Smirnov test was used to assess goodness of fit of alternative two-parameter distributions applied to experimental data. Lastly, the Kruskal-Wallis (Kruskal and Wallis. 1952) and the Wilcoxon signed-rank tests (Wilcoxon. 1945) were used to compare distributions. Statistical significance was considered to be  $p < 0.05$ .

### *Results*

#### *First approach to determining elastic modulus: Hertz's single contact and Theret's models*

AFM force (F)-displacement ( $\delta$ ) data were initially fitted to Hertz's classical single contact model. As may be seen in Figure 4a, there is reasonable accordance between the experimental data and the model predictions, showing

the non-linear behavior of the force-displacement curve. The elastic modulus ( $E$ ) was obtained by a least-squares fit to the equation shown in Table 1. Data from MPA were initially analyzed with Theret's classical model expression. A representative curve is shown in Figure 4b. Cellular deformation is expressed as the ratio between the length of the cell that enters the micropipette,  $L$ , and the micropipette radius,  $R_p$  and is represented as a function of suction pressure  $\Delta P$ . By using Theret's model (Table 1), a value for the elastic modulus of the lymphocytes can be deduced from fitting to MPA data. A initial experimental difference between the techniques is related to the number of cells that may be tested at equal processing times. MPA has a much higher throughput compared with AFM, so more than 300 cells were analyzed in the MPA experiments, compared with 20 cells studied by AFM in a time-frame of 100 hours. Another major difference is that each cell is sampled only once in MPA tests while several force-displacement curves (at least 30) may be obtained from each cell by using AFM. In order to account for the possible effect related with the different number of cells tested with each technique, groups of 20 curves corresponding to MPA experiments were randomly selected and the distribution of their elastic moduli were compared with the whole set of curves. No significant statistical differences between the distribution of smaller sets and that including all the curves were observed (p-value = 0.08 in the Kruskal-Wallis test).

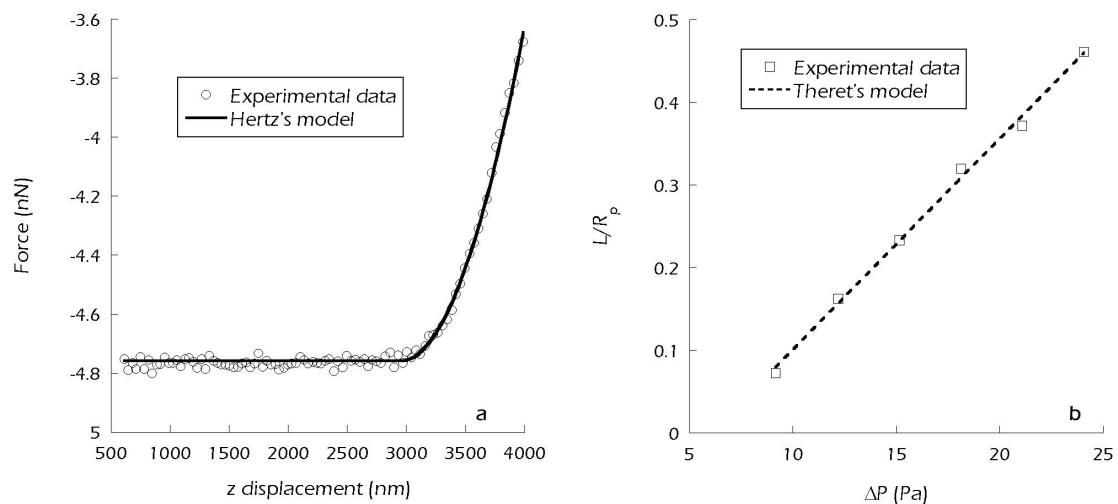


Figure 4. (a) Representative experimental force-displacement curve measured on a T lymphocyte with AFM (circles). The solid line shows the fit to Hertz's model. (b) Representative result of an MPA test representing cell deformation as a function of suction pressure. The dashed line shows fit to Theret's model.

Figure 5 shows the histograms for the values of elastic moduli obtained from Hertz's and Theret's models. A summary of the main statistical parameters describing distributions is shown in Table 2.

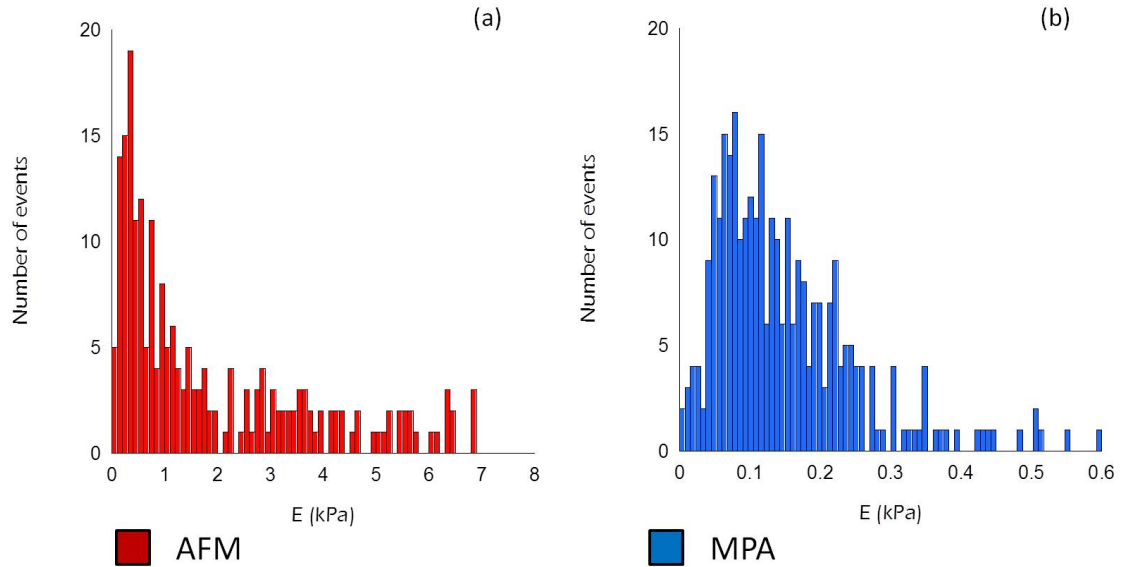


Figure 5. Elastic moduli values calculated from analyzing the experimental AFM and MPA data using the Hertz (a) and Theret (b) models.

From Figure 5 and Table 2 it is apparent the quantitative and qualitative differences found between both distributions of elastic moduli.

**TABLE 2. Statistical parameters associated with histograms of Figure 3**

	Mean (kPa)	Median (kPa)	Std. deviation (kPa)	Std. error (kPa)	Relative error	Skewness	Kurtosis
AFM	1.900	1.000	2.026	0.100	0.05	1.869	5.775
MPA	0.149	0.124	0.102	0.007	0.04	1.514	3.208

Both distributions present comparable relative errors (4-5%) despite the significant difference in the number of cells characterized. Furthermore, both distributions show non-zero skewness values which reflects the lack of symmetry. Kurtosis values above three suggest that the data distribution may differ from a Gaussian function.

In order to obtain a quantitative evaluation of the divergence between MPA and AFM distributions from a Gaussian function, both Kolmogorov-Smirnov and

Shapiro-Wilk tests were used. As Figure 5 suggests, there is a clear divergence from Gaussian distribution given by both tests (p-values < 0.05). Consequently, alternative distributions (such as t-student, triangular, Rayleigh, Maxwell, log-normal, logistic, Cauchy or Erlang distributions) were considered to describe the experimental data and their validity was tested by means of the Kolmogorov-Smirnov test.

It was found that the Gamma distribution fits the experimental data with reasonable precision. The Kolmogorov-Smirnov test rendered p-values of 0.95 for both MPA and AFM data. Table 3 shows the expressions corresponding a Gamma statistical distribution as a function of the parameters: shape ( $\alpha$ ) and scale ( $\beta$ ).

**TABLE 3. Probability density function (PDF) and the cumulative distribution function (CDF) for a Gamma distribution.  $\Gamma(\alpha) = (\alpha - 1)!$  is the Gamma function.**

Gamma	
PDF	$f(x; \alpha, \beta) = \frac{1}{\beta^\alpha \Gamma(\alpha)} x^{\alpha-1} e^{-x/\beta}$
CDF	$F(x; \alpha, \beta) = \frac{1}{\beta^\alpha \Gamma(\alpha)} \int_0^x t^{\alpha-1} e^{-t/\beta} dt$

Gamma cumulative distribution functions for the experimental data are shown in Figure 6a and Figure 6b.

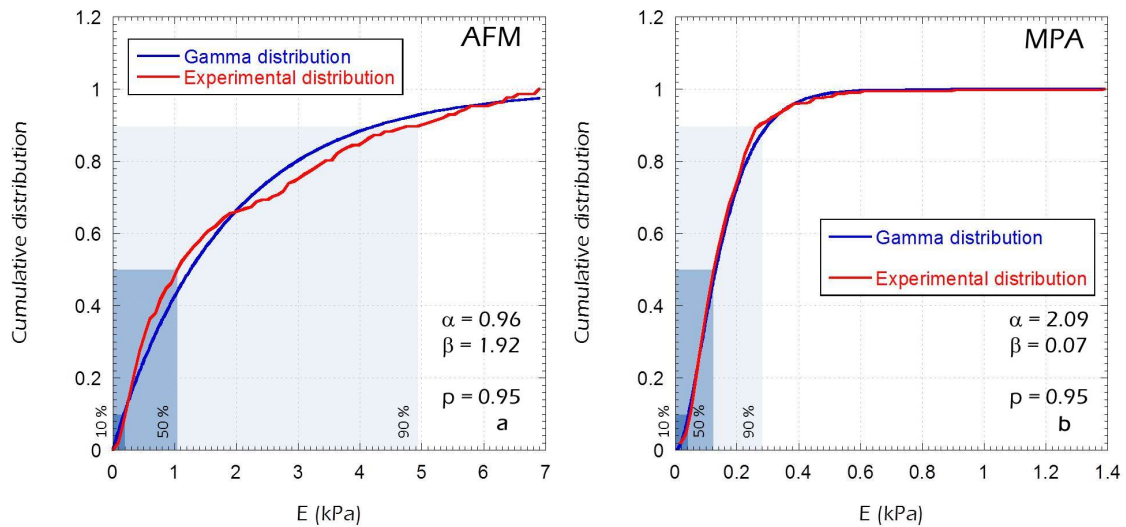


Figure 6. Cumulative Gamma distribution functions for the AFM (a) and MPA (b) experimental data. Shaded areas indicate intervals for 10, 50 and 90% probability.

Figure 6 confirms that MPA and AFM data can be fitted to a Gamma distribution, despite significant quantitative differences in the predicted elastic moduli.

Considerable differences in elastic moduli between MPA and AFM data were confirmed by the Kruskal-Wallis test and the Wilcoxon signed-rank test. Both tests yielded extremely low values of  $p$  (0.001 and 0.004, respectively).

*Second approach to determining elastic moduli: SDC and Zhou's models*

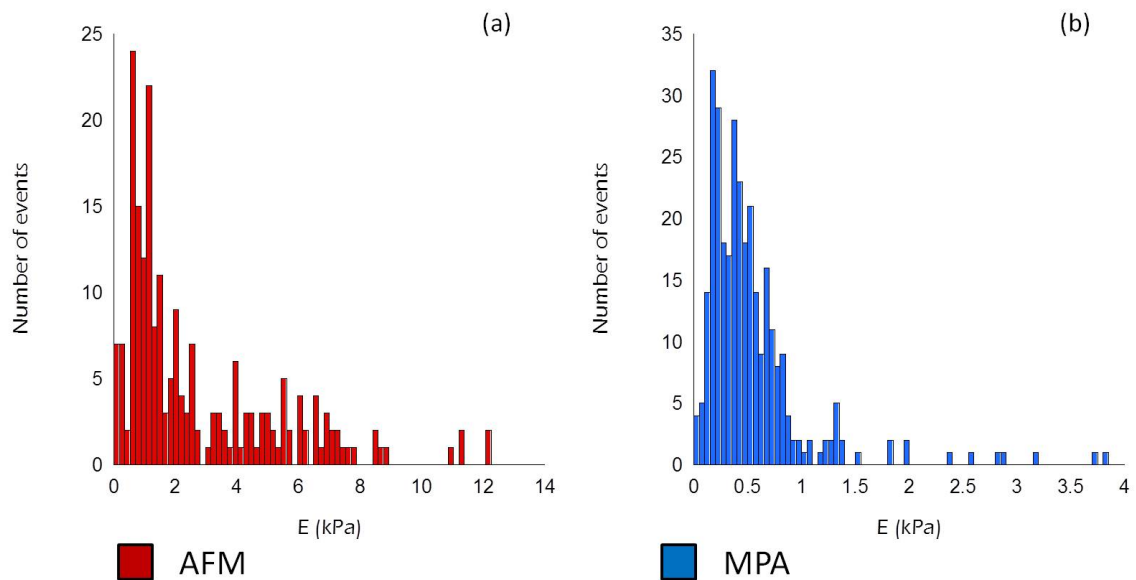


Figure 7. Elastic moduli distributions from analyzing experimental AFM and MPA data by means of the SDC (a) and Zhou (b) models.

As shown above, the analysis was refined by considering other possible theoretical models, such as the simplified double contact (SDC) model for AFM data (Glaubitz et al. 2014) and Zhou's model for MPA measurements. Both models take into account the finite size of the cell, with the SDC model considering substrate-cell contact.

Figure 7 shows the histograms for elastic moduli and Table 4 summarizes the main statistical parameters. Both distributions again show high skewness values, which suggest a non-Gaussian distribution. This non-Gaussian behavior

was confirmed by p-values (0.001 and 0.0002) in the Kolmogorov-Smirnov and Shapiro-Wilk tests. Following prior analysis, data were fitted to non-symmetric, two-parameter distributions and, although MPA data could be appropriately fitted to a Gamma distribution (Figure 8b), AFM did not fit to Gamma or any other common two-parameter statistical distribution (Figure 8a).

**TABLE 4. Statistical parameters of the distributions of elastic moduli calculated from the experimental data using Zhou and SDC models.**

	Mean (kPa)	Median (kPa)	Std. deviation (kPa)	Std. error (kPa)	Relative error	Skewness	Kurtosis
AFM	2.7	1.5	2.6	0.2	0.07	1.4	1.7
MPA	0.5	0.4	0.5	0.03	0.06	3.4	15.2

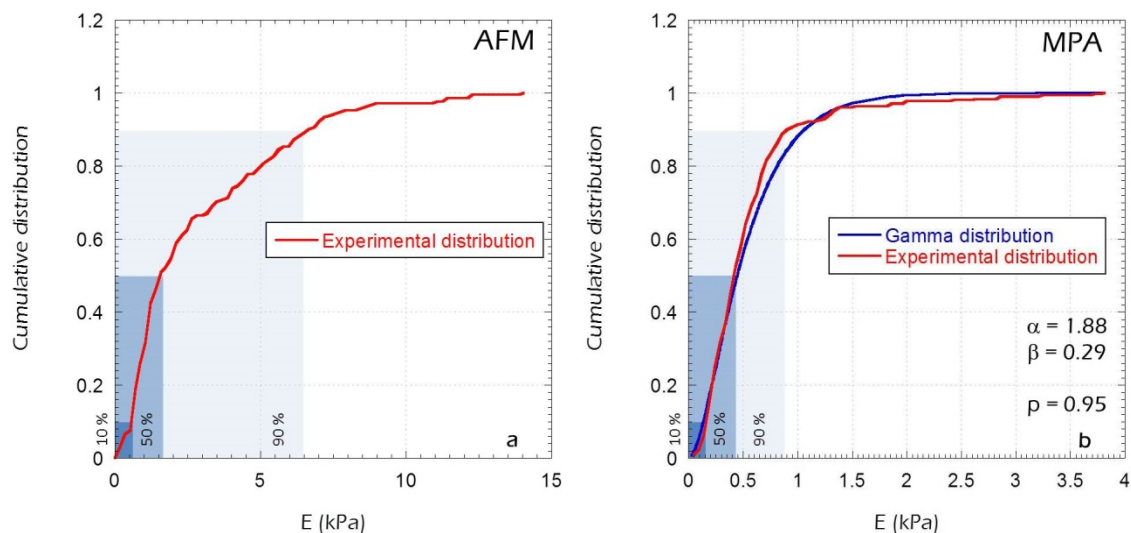


Figure 8. Cumulative distribution functions for the (a) AFM-SDCM and (b) MPA-Zhou experimental data and fitting obtained considering a Gaussian distribution function. Shaded zones indicate the elastic moduli intervals with a 10, 50 and 90% probability.

### *Geometrical distribution of the cytoskeleton components*

Figure 9 shows a reconstruction of the geometry of a lymphocyte adhered to a biofunctionalized substrate as used for AFM measurements. The images show that the lymphocyte presents a spherical geometry with only limited flattening in the region of contact with the substrate. In addition, it is possible to observe that actin fibers (in red) are circumferentially distributed.



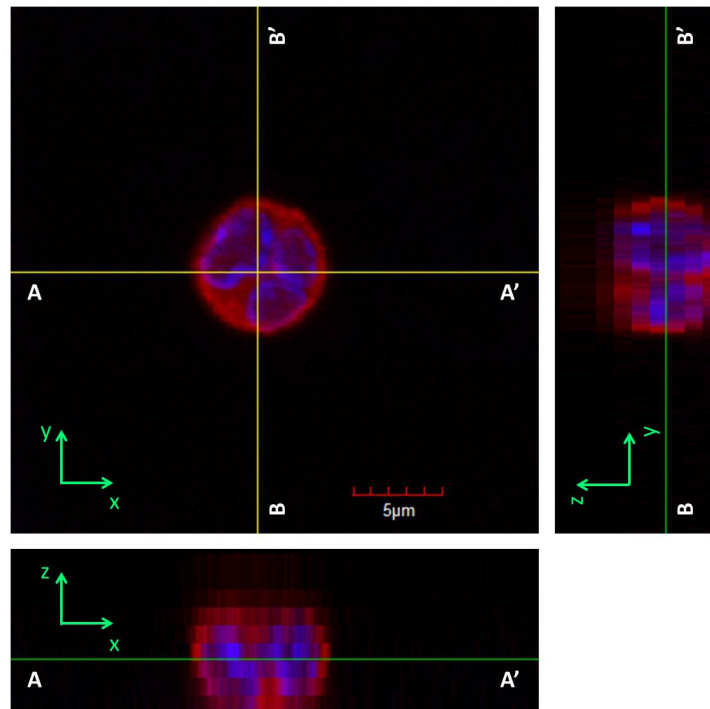


Figure 9. Representative confocal XZ and YZ profiles (Z-scans) of a T-lymphocyte adhered to a biofunctionalized substrate. In blue, it is possible to observe the nucleus, while the actin fibers are shown in red.

Confocal images allowed us to recognize heterogeneous distribution of the chromatin in the cellular nucleus as may be seen in the left-hand images of Figure 10, showing two different T-lymphocytes nucleus stained with DAPI.

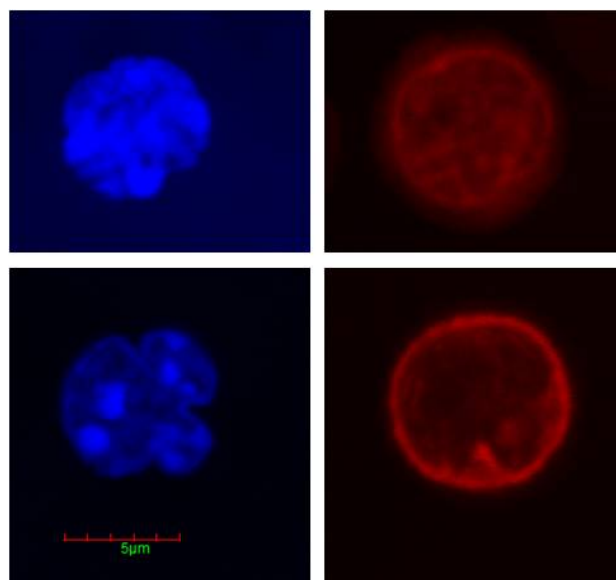


Figure 10. Confocal images of two T lymphocytes. The images on the left show the DNA inhomogeneous compacting grade (dark and pale blue which correspond with heterochromatin and euchromatin, respectively) whereas those on the right depict the cell cytoplasm.

## *Discussion*

Several studies have established that the mechanical properties of cells are useful markers of cell state. Furthermore, the deformability of cells is a promising biomarker for various disease processes and changes in cell state and is understood to be associated with cytoskeletal and nuclear changes (Suresh. 2007, Suresh et al. 2005, Ingber. 2003, Zhu et al. 2000, Stewart et al. 2011). Mechanical deformability is particularly important in cell migration, which plays a vital role in a large number of cells, including blood and immune cells. In this regard, it is well established that the activity of cells such as red blood cells or lymphocytes depend on the ability to flow through narrow channels. The development of different experimental techniques for assessing the mechanical properties of cells imply that large variations are usually found when comparing data obtained, depending on the technique used for characterization. This issue entails a significant drawback in any attempt to standardize the experimental data. Therefore, it would be extremely helpful if the principles that underlie these discrepancies were identified and compensated.

T-lymphocytes are cells that determine the specificity of the immune response to infectious microorganisms. T-lymphocytes mature in the thymus (Zdrojewicz et al. 2016, Carpenter and Bosselut. 2010) and are subsequently released into the circulatory system where they remain circulating until recognition of their specific antigen. Therefore, T-lymphocytes do not attach themselves to most surfaces (Gupta et al. 1999), simplifying their isolation from other immune cells (Russo et al. 1979) and allowing them to flow into the pipette, but hampering their AFM observation where cell immobilization is a pre-requisite. Consequently, many AFM studies on lymphocytes use cell fixation procedures, despite possible alterations involved in these methods. In a previous work, the authors developed a procedure which allowed immobilization of T-Lymphocytes without fixing them and without observing any modification of their original rounded shape or their non-activated state (Daza et al. 2015). Accordingly, T-Lymphocytes represent a suitable system for comparing results obtained by MPA and AFM due to their low adherence to the substrate (except on

specifically engineered substrates) and the lack of variations in their geometry upon immobilization on a substrate.

Nevertheless, the mechanical properties of T-lymphocytes as measured by MPA and AFM techniques report significant differences in their results, in some cases even greater than an order of magnitude. The same trend has been observed when mechanically characterizing other biological entities by means of MPA and AFM.

Special importance was assigned to the theoretical model used to calculate the value of the elastic moduli from the experimental data. Initially, the data provided by MPA and AFM were analyzed by using the Theret's and Hertz's classical models, which considered semi-infinite samples. Figure 5 shows that the calculated elastic moduli distribution exhibited an evident non-normal distribution as later verified by Kolmogorov-Smirnov's and Shapiro-Wilk's tests. Divergence of these data from a Gaussian distribution seems to be related with the existence of tails in the range of high values of the elastic moduli.

After a number of trials, it was found that the experimental data could be fitted to a Gamma distribution. Gamma distribution has been used for modeling different biological processes. Thus, Maloney et al. demonstrated that cell compliance varies according to a gamma distribution (Oyen. 2010). Yu et al. modeled the process of stochastic protein production (Yu et al. 2006) and other published authors considered a gamma distribution to describe the protein content in bacteria and other organisms (Ray. 2016, Coroller et al. 2006).

Quantitative analysis of the data shows that the elastic moduli calculated from AFM data are significantly higher than those obtained from MPA data. It is also observed that the discrepancy between the elastic moduli determined from both techniques is less when medians are compared instead of mean values. The lower values of the elastic moduli obtained from MPA data compared with AFM data were reported from other cell lineages. For instance, Darling et al. (Darling et al. 2006) reported that values provided by MPA were 35% lower than those estimated by AFM. Dahl et al. (Dahl et al. 2005) also found that MPA data tended to be 50 % less than data from AFM.

In order to refine the results, some theoretical models that take into account the finite size of the cells were then applied. Zhou's model for MPA and the SDC model for AFM yielded new distribution functions with closer values of the elastic moduli. The new distribution functions did not correspond to the Gaussian functions either, but data obtained from MPA fitted a Gamma distribution. Nevertheless, no ordinary two-parameter statistical distribution could fit the AFM data. In both experiment types, models considering the finite size of cells rendered higher values of the elastic moduli.

The use of refined models reduces the difference between the elastic moduli obtained, especially when comparing median values (Table 4), which differ by a factor of three (in contrast to a ratio greater than seven for simple models). Consequently, although consideration of the finite sample size did not resolve inconsistency between the elastic moduli distributions (Figure 7), the differences between them are significantly reduced.

It is worth considering other possible causes for the discrepancy of values obtained from MPA and AFM apart from finite cell size. The first issue we should consider is the suitability of using elastic models to analyze the mechanical behavior of cells, which have been broadly characterized as viscoelastic materials (Trepap et al. 2007, Nawaz et al. 2012). Lim and collaborators (Lim et al. 2006) addressed this question and reported that elastic analysis is inappropriate to describe cell mechanics, because the apparent elastic moduli measured in viscoelastic materials depends on loading rates and previous loading history. However, such apparent elastic moduli could be used as a pillar for a viscoelastic solution to the problem by using the correspondence principle (Fung. 1965). In this respect, we consider comparison between both techniques to be easier if only one parameter, i.e. elastic modulus, must be analyzed. The different loading-rate characteristics of MPA and AFM tests, together with their viscoelastic behavior, could justify part of the discrepancies observed in measured elastic parameters (since force displacement curves were carried out at  $1 \mu\text{m s}^{-1}$ , the loading rate in AFM measurements was slightly faster when compared with the loading of MPA experiments ( $0.1 \mu\text{m s}^{-1}$ ). Different authors have characterized the apparent

elastic modulus of cells when indented by AFM at different loading rates. Li and collaborators (Li et al. 2008) reported a twofold variation of elastic modulus when the loading rate was increased by thirty. Nguyen (Trung Dung Nguyen and Gu. 2014) observed that the maximum applied force over osteocytes reduced from around 6.73 to 1.55 nN with drop in strain rate from 7.4 to 0.0123 Hz, demonstrating the reduction in cell stiffness. Recently, Zhou and collaborators (Zhou et al. 2012) found a growth in elastic modulus value from 2 kPa to 10 kPa when the loading rate was increased from 0.1 to 1.1  $\mu\text{m s}^{-1}$  in UM1 oral cancer cells. Caporizzo (Caporizzo et al. 2015), working with three different types of cells, found that the evolution of their elastic moduli, measured at different loading rates and fitted using Hertz's model, could be perfectly simulated by the solid elastic simple model (SLSM). This model establishes the presence of plateaus in elastic modulus behavior at low and at high frequencies. In this respect, HUVEC cells were found to exhibit a plateau around 0.7 kPa at low frequencies and another near 1.5 kPa at high rates. Using the same model for measurements made with MPA, Pravin Kumar and collaborators (Pravin Kumar et al. 2012) observed that the higher the rate of pressure applied, the more flexible the cells behaved.

In addition to the possible effect of the viscoelastic behavior of the cells, previous studies have assessed the influence of the different boundary conditions imposed on cells by both techniques. Use of MPA requires the cell to be detached from the substrate. Conversely, measuring the mechanical properties of the cell by AFM requires that the cell remains immobilized on a substrate. In this regard, Bacabac et al. (Bacabac et al. 2008) used AFM to measure the mechanical behavior of osteocytes as a function of force of adhesion to the substrate and found differences higher than an order of magnitude in the elastic moduli. Osteocytes more adhered to the substrate have a tendency to show a higher elastic modulus. Additionally, Genes et al. (Genes et al. 2004) established that flat cellular morphology is maintained by pre-stressed fiber bundles, while spherical cells retain their geometry due to a combination of high surface tension and osmotic pressure. This model is consistent with an increase in the elastic modulus of cells adhered to a substrate, related with an increase in the density of cytoskeletal fibrils.

Furthermore, by using purely geometrical considerations and finite model analysis, Vichare et al. (Vichare et al. 2012) showed that Hertz's model overestimates elastic modulus values when spread cells are considered. In order to examine the possible effect of adherence to a substrate in our results, the study analyzed the geometry of T-lymphocytes, as well as the possible increase in the density of cytoskeletal fibrils in the vicinity of the substrate by means of confocal microscopy images.

Figure 9 shows a reconstruction of the geometry of a lymphocyte adhered to a biofunctionalized substrate as used for AFM measurements. The images show that the lymphocyte presents a spherical geometry with only a small flattening in the region of contact with the substrate. Use of rhodamine-phalloidin dye allows a homogenous circumferential distribution of fibrils in the cell to be observed, with no particular increase of cytoskeletal fibers in the contact region detected. These results suggest, at least for T-lymphocytes, that the discrepancies in elastic moduli found between AFM and MPA techniques do not seem to be a consequence of adhesion of the cells to the substrate and subsequent remodeling of their cytoskeleton. Such an effect, however, may be relevant for other cell lineages with a flatter geometry when adhered to a surface.

Another possible contribution to the variances in the mechanical parameters measured by MPA and AFM is the different distribution of stresses induced in the cell by both techniques. In this regard, a first difference can be established between the volume of the cell relevant to the experiment. This volume can be considered to be proportional to the indentation depth ( $\delta$ ) for AFM and to the length of cell inside the micropipette ( $L$ ) for MPA measurements. Therefore, in order to reduce the effect of this possible source of discrepancy, only indentations and lengths of cell inside the micropipette less than 1  $\mu\text{m}$  (which implies deformations of less than 10% of the characteristic size of these cells) were considered (as may be plausibly inferred from the graphs showed in Figure 4). However, even the consideration of similar values of  $\delta$  and  $L$  cannot circumvent the local character of AFM measurements, in clear contrast with the global nature of MPA where, in addition, there is a region of large deformation at the edges of the micropipette. Local effects might be even more significant if

pyramidal and not spherical tips are used. Spherical tips reduce local stress at the contact point. Although pyramidal tips lead to a higher stress concentration, this type of tip offers the possibility of obtaining high-resolution images of the cell in addition to mechanical data. Significant differences were found in the elastic modulus values of cells and gels, depending on whether spherical or pyramidal tips were used as sensors. Thus, Rico et al. (Rico et al. 2005) reported that the elastic moduli of agarose gels and alveolar epithelial cells were doubled when they were measured by means of pyramidal tips compared with the values obtained from spherical tips. Similarly, Guz et al. (Guz et al. 2014) obtained a ratio between human epithelial cell elastic moduli measured by pyramidal and spherical tip higher than five. Usage of pyramidal tips might account partly for the differences observed between MPA and AFM data. However, other authors have reported discrepancies between both techniques even when using spherical tips (Dahl et al. 2005, Darling et al. 2006).

Lastly, the possible influence of inhomogeneity of the cells was considered. An example of these inhomogeneities is shown in Figure 10. In this case, inhomogeneity is associated with the different organization of DNA as either heterochromatin or euchromatin. As other authors have reported, these configurations may exhibit different mechanical behavior (Dahl et al. 2005, Pajerowski et al. 2007) the local character of AFM measurements may be affected by this source of inhomogeneity or by others related with spatial organization of the cytoskeleton: the existence of these inhomogeneities could be detected by AFM measurements, but would be averaged out with global MPA measurements.

## Conclusions

A comparative analysis of the mechanical data obtained from MPA and AFM has been presented. The results obtained by fitting the experimental data to the simple Hertz (for AFM) and Theret (for MPA) models lead to non-Gaussian distributions, and significantly higher elastic moduli were obtained from the AFM data. The use of more refined models that take into account finite size of the cells yields values closer to elastic moduli. However, there remains a substantial three-fold factor between mean values obtained by both techniques.

Three possible sources for the discrepancy between both techniques were considered. (1) The viscoelastic behavior of cells, (2) changes in the cell cytoskeleton upon adhering to a substrate and (3) inhomogeneities in the cytoskeleton of the cell. Analysis of each of these contributions shows that the higher strain rate of AFM measurements compared with MPA justifies an increase in the apparent elastic modulus calculated from AFM data. In addition, possible inhomogeneities in the cytoskeleton are more likely to influence the local AFM measurements than the more holistic MPA measurements. Lastly, preliminary analysis of the organization of the cytoskeleton around the contact point to the surface in lymphocytes did not find any significant disturbance in this organization. Such reorganization, however, might be more relevant for cells with greater differences in geometry between adhered and non-adhered states.

#### Acknowledgments

Dr. A. Gil and L. Colchero (Nanotec Electrónica, S.L., Spain) provided support for AFM observations and E. Baldonado (Centro de Microscopía, UCM, Spain) for confocal observations. The authors are grateful to José Miguel Martínez for his help with the artwork. The authors also gratefully acknowledge financial support received from the Ministerio de Economía y Competitividad in Spain through grants MAT2016-76847-R and MAT2016-79832-R, and Comunidad de Madrid through grant Neurocentro-B2017/BMD-3760.



## APPENDIX

### Kolmogorov-Smirnov test

The Kolmogorov-Smirnov test is used to decide whether a sample comes from a population with a specific distribution or to compare two distributions. It is based on the maximum vertical distance between an empirical distribution function EDF from an experimental sample and the cumulative distribution function CDF of a known distribution. Given  $N$  ordered data points  $Y_1, Y_2, \dots, Y_N$ , the EDF is defined as:

$$E_n = \frac{n(i)}{N}$$

where  $n(i)$  is the number of points with values less than  $Y_i$ , being  $Y_i$  values ordered from smallest to largest. This is a step function that increases by  $1/N$  at the value of each ordered data point.

The Kolmogorov-Smirnov test is defined by:

$H_0$ : The data follow a specified distribution

$H_a$ : The data do not follow the specified distribution

Test Statistic: The Kolmogorov-Smirnov test statistic is defined as

$$T = \max_{1 \leq i \leq N} \left\{ F(Y_i) - \frac{i-1}{N}, \frac{i}{N} - F(Y_i) \right\}$$

where  $F$  is the theoretical cumulative distribution of the distribution being tested. If  $T$  exceeds the  $1-p$  quantile as given by the table of quantiles for the Kolmogorov test statistic, then we reject  $H_0$  at the level of significance  $p$  (Conover, 1971).

## References

Allen DM, Mao JJ. Heterogeneous nanostructural and nanoelastic properties of pericellular and interterritorial matrices of chondrocytes by atomic force microscopy. *J.Struct.Biol.* 2004 MAR 2004;145(3):196-204.

Arroyo-Hernandez M, Daza R, Perez-Rigueiro J, Elices M, Nieto-Marquez J, Guinea GV. Optimization of functionalization conditions for protein analysis by AFM. *Appl.Surf.Sci.* 2014 OCT 30 2014;317:462-8.

Bacabac RG, Mizuno D, Schmidt CF, MacKintosh FC, Van Loon JJWA, Klein-Nulend J, et al. Round versus flat: Bone cell morphology, elasticity, and mechanosensing. *J.Biomech.* 2008;41(7):1590-8.

Bader D, Ohashi T, Knight M, Lee D, Sato M. Deformation properties of articular chondrocytes: A critique of three separate techniques. *Biorheology* 2002;39(1-2):69-78.

Binnig G, Quate CF, Gerber C. Atomic Force Microscope. *Phys.Rev.Lett.* 1986 MAR 3 1986;56(9):930-3.

Caporizzo MA, Roco CM, Ferrer MCC, Grady ME, Parrish E, Eckmann DM, et al. Strain-rate Dependence of Elastic Modulus Reveals Silver Nanoparticle Induced Cytotoxicity. 2015 2018/11;2:9.

Carpenter AC, Bosselut R. Decision checkpoints in the thymus. *Nat.Immunol.* 2010 AUG;11(8):666-73.

Conover WJ. *Practical Nonparametric Statistics.* : John Wiley & Sons; 1971.

Coroller L, Leguerinel I, Mettler E, Savy N, Mafart P. General model, based on two mixed Weibull distributions of bacterial resistance, for describing various shapes of inactivation curves. *Appl.Environ.Microbiol.* 2006 OCT;72(10):6493-502.

Costa KD. Imaging and probing cell mechanical properties with the atomic force microscope. *Methods Mol.Biol.* 2006 2006;319:331-61.

Dahl K, Engler A, Pajerowski J, Discher D. Power-law rheology of isolated nuclei with deformation mapping of nuclear substructures. *Biophys.J.* 2005 OCT;89(4):2855-64.

Darling E, Zauscher S, Guilak F. Viscoelastic properties of zonal articular chondrocytes measured by atomic force microscopy. *Osteoarthritis and Cartilage* 2006 JUN;14(6):571-9.

Daza R, Cruces J, Arroyo-Hernandez M, Mari-Buye N, De la Fuente M, Plaza GR, et al. Topographical and mechanical characterization of living eukaryotic cells on opaque substrates: development of a general procedure and its

application to the study of non-adherent lymphocytes. *Physical biology* 2015 2015 Apr;12(2):026005.

de Pablo PJ, Colchero J, Gomez-Herrero J, Baro AM. Jumping mode scanning force microscopy. *Appl.Phys.Lett.* 1998 NOV 30 1998;73(22):3300-2.

Derganc J, Bozic B, Svetina S, Zeks B. Stability analysis of micropipette aspiration of neutrophils. *Biophys.J.* 2000 JUL;79(1):153-62.

Dimitriadis EK, Horkay F, Maresca J, Kachar B, Chadwick RS. Determination of elastic moduli of thin layers of soft material using the atomic force microscope. *Biophys.J.* 2002 MAY 2002;82(5):2798-810.

Dulińska I, Targosz M, Strojny W, Lekka M, Czuba P, Balwierz W, et al. Stiffness of normal and pathological erythrocytes studied by means of atomic force microscopy. *J.Biochem.Biophys.Methods* 2006 3/31;66(1–3):1-11.

Esteban-Manzanares G, González-Bermúdez B, Cruces J, De IF, Li Q, Guinea GV, et al. Improved Measurement of Elastic Properties of Cells by Micropipette Aspiration and Its Application to Lymphocytes. *Ann.Biomed.Eng.* 2017:1-11.

Florea C, Jakorinne A, Lammi M, Davidescu A, Korhonen RK. Determination of Mechanical Properties of Chondrocytes in Articular Cartilage using Atomic Force Microscopy. *Advanced Materials and Structures V* 2014 2014;216:134-9.

Fung Y. *Foundations of solid mechanics.* Englewood Cliffs, New Jersey: Englewood Cliffs, New Jersey Prentice-Hall; 1965.

Genes N, Rowley J, Mooney D, Bonassar L. Effect of substrate mechanics on chondrocyte adhesion to modified alginate surfaces. *Arch.Biochem.Biophys.* 2004 FEB 15;422(2):161-7.

Glaubitz M, Medvedev N, Pussak D, Hartmann L, Schmidt S, Helm CA, et al. A novel contact model for AFM indentation experiments on soft spherical cell-like particles. *Soft Matter* 2014;10(35):6732-41.

Guilak F, Trickey WR, Baaijens FPT, Laursen TA, Alexopoulos LG. Determination of the Poisson's ratio of the cell: recovery properties of chondrocytes after release from complete micropipette aspiration. *J.Biomech.* 2006 2006;39(1):78-87.

Gupta S, Aggarwal S, Starr A. Increased production of interleukin-6 by adherent and non-adherent mononuclear cells during 'natural fatigue' but not following 'experimental fatigue' in patients with chronic fatigue syndrome. *Int.J.Mol.Med.* 1999 FEB 1999;3(2):209-13.

Guz N, Dokukin M, Kalaparathi V, Sokolov I. If Cell Mechanics Can Be Described by Elastic Modulus: Study of Different Models and Probes Used in Indentation Experiments. *Biophys.J.* 2014 AUG 5;107(3):564-75.

Hertz H. On the contact of elastic solids. In: Lenard P, editor. Miscellaneous papers; 1896. p. 146.

Hertz H. Über die berührung fester elastischerkörper. 1882;92:156.

Horcas I, Fernandez R, Gomez-Rodriguez JM, Colchero J, Gomez-Herrero J, Baro AM. WSXM: A software for scanning probe microscopy and a tool for nanotechnology. Rev.Sci.Instrum. 2007 JAN 2007;78(1):013705.

Ingber D. Mechanobiology and diseases of mechanotransduction. Ann.Med. 2003;35(8):564-77.

Jansen KA, Donato DM, Balcioglu HE, Schmidt T, Danen EHJ, Koenderink GH. A guide to mechanobiology: Where biology and physics meet. Biochim.Biophys.Acta 2015 2015 Nov (Epub 2015 May 18);1853(11 Pt B):3043-52.

Jiao GY, Tan KSW, Sow CH, Dao M, Suresh S, Lim CT. Computational Modeling of the Micropipette Aspiration of Malaria Infected Erythrocytes. 13th International Conference on Biomedical Engineering, Vols 1-3 2009;23(1-3):1788-91.

Kruskal W, Wallis W. Use of Ranks in One-Criterion Variance Analysis. Journal of the American Statistical Association 1952;47(260):583-621.

Li QS, Lee GYH, Ong CN, Lim CT. AFM indentation study of breast cancer cells. Biochem.Biophys.Res.Commun. 2008 OCT 3;374(4):609-13.

Lim C, Zhou E, Quek S. Mechanical models for living cells - A review. J.Biomech. 2006;39(2):195-216.

Massey F. The Kolmogorov-Smirnov Test for Goodness of Fit. J.Am.Stat.Assoc. 1951;46(253):68-78.

Mitchison J, Swann M. The Mechanical Properties of the Cell Surface .1. the Cell Elastimeter. J.Exp.Biol. 1954;31(3):443-61.

Moreno-Herrero F, Colchero J, Gomez-Herrero J, Baro A. Atomic force microscopy contact, tapping, and jumping modes for imaging biological samples in liquids. Physical Review E 2004 MAR;69(3):031915.

Nawaz S, Sanchez P, Bodensiek K, Li S, Simons M, Schaap IAT. Cell Visco-Elasticity Measured with AFM and Optical Trapping at Sub-Micrometer Deformations. PLoS One 2012 SEP 19;7(9):e45297.

Oyen M. Handbook of Nanoindentation with Biological Applications. SINGAPORE; PENTHOUSE LEVEL, SUNTEC TOWER 3, 8 TEMASEK BLVD, SINGAPORE, 038988, SINGAPORE: PAN STANFORD PUBLISHING PTE LTD; 2010.

Öztuna D, Atilla HE, Tüccar E. Investigation of Four Different Normality Tests in Terms of Type 1 Error Rate and Power under Different Distributions. Turkish Journal of Medical Sciences 2006 06;36(3):171-6.

Pajeroski JD, Dahl KN, Zhong FL, Sammak PJ, Discher DE. Physical plasticity of the nucleus in stem cell differentiation. Proc.Natl.Acad.Sci.U.S.A. 2007 OCT 2;104(40):15619-24.

Plaza GR, Mari N, Galvez BG, Bernal A, Guinea GV, Daza R, et al. Simple measurement of the apparent viscosity of a cell from only one picture: Application to cardiac stem cells. Physical Review E 2014 NOV 17;90(5):052715.

Pravincumar P, Bader DL, Knight MM. Viscoelastic Cell Mechanics and Actin Remodelling Are Dependent on the Rate of Applied Pressure. PLoS One 2012 SEP 11;7(9):e43938.

Rand R, Burton A. Mechanical Properties of Red Cell Membrane .I. Membrane Stiffness + Intracellular Pressure. Biophys.J. 1964;4(2):115.

Ray JCJ. Survival of Phenotypic Information during Cellular Growth Transitions. Acs Synthetic Biology 2016 AUG;5(8):810-6.

Rico F, Roca-Cusachs P, Gavara N, Farre R, Rotger M, Navajas D. Probing mechanical properties of living cells by atomic force microscopy with blunted pyramidal cantilever tips. Physical Review E 2005 AUG 2005;72(2):021914.

Roca-Cusachs P, Almendros I, Sunyer R, Gavara N, Farre R, Navajas D. Rheology of passive and adhesion-activated neutrophils probed by atomic force microscopy. Biophys.J. 2006 NOV;91(9):3508-18.

Rosenbluth M, Lam W, Fletcher D. Force microscopy of nonadherent cells: A comparison of leukemia cell deformability. Biophys.J. 2006 APR;90(8):2994-3003.

Russo AJ, Howell JH, Han T, Bealmear P, Goldrosen MH. Isolation of T-Cells, B-Cells and Macrophages by a 2-Stage Adherence Procedure. J.Clin.Lab.Immunol. 1979 1979;2(1):67-72.

Sader JE, Chon JWM, Mulvaney P. Calibration of rectangular atomic force microscope cantilevers. Rev.Sci.Instrum. 1999 OCT 1999;70(10):3967-9.

Schillers H, Rianna C, Schaepe J, Luque T, Doschke H, Waelte M, et al. Standardized Nanomechanical Atomic Force Microscopy Procedure (SNAP) for Measuring Soft and Biological Samples. Sci Rep 2017 JUL 11;7:5117.

Schmidtschonbein G, Sung K, Tozeren H, Skalak R, Chien S. Passive Mechanical-Properties of Human-Leukocytes. Biophys.J. 1981;36(1):243-56.

Schneider S, Zilow E, Linderkamp O. Estimation of Deformability of Neonatal and Adult Leukocytes Via Micropipette Aspiration. *Pediatr.Res.* 1987 AUG 1987;22(2):219-.

Shapiro S, Francia R. Approximate Analysis of Variance Test for Normality. *J.Am.Stat.Assoc.* 1972;67(337):215.

Shapiro S, Wilk M. An Analysis of Variance Test for Normality (Complete Samples). *Biometrika* 1965;52:591.

Stewart MP, Toyoda Y, Hyman AA, Muller DJ. Force probing cell shape changes to molecular resolution. *Trends Biochem.Sci.* 2011 8;36(8):444-50.

Suresh S, Spatz J, Mills J, Micoulet A, Dao M, Lim C, et al. Connections between single-cell biomechanics and human disease states: gastrointestinal cancer and malaria. *Acta Biomaterialia* 2005 JAN;1(1):15-30.

Suresh S. Biomechanics and biophysics of cancer cells. *Acta Biomaterialia* 2007 JUL;3(4):413-38.

Theret D, Levesque M, Sato M, Nerem R, Wheeler L. The Application of a Homogeneous Half-Space Model in the Analysis of Endothelial-Cell Micropipette Measurements. *Journal of Biomechanical Engineering-Transactions of the Asme* 1988 AUG;110(3):190-9.

Trepats X, Deng L, An SS, Navajas D, Tschumperlin DJ, Gerthoffer WT, et al. Universal physical responses to stretch in the living cell. *Nature* 2007 MAY 31;447(7144):592.

Trung Dung Nguyen, Gu Y. Determination of Strain-Rate-Dependent Mechanical Behavior of Living and Fixed Osteocytes and Chondrocytes Using Atomic Force Microscopy and Inverse Finite Element Analysis. *J.Biomech.Eng.-Trans.ASME* 2014 OCT;136(10):101004.

Vichare S, Inamdar MM, Sen S. Influence of cell spreading and contractility on stiffness measurements using AFM. *Soft Matter* 2012;8(40):10464-71.

Wang J, Thampatty B. An introductory review of cell mechanobiology. *Biomechanics and Modeling in Mechanobiology* 2006 MAR;5(1):1-16.

Wilcoxon F. Individual Comparisons by Ranking Methods. *Biometrics Bulletin* 1945;1(6):80-3.

Yu J, Xiao J, Ren X, Lao K, Xie X. Probing gene expression in live cells, one protein molecule at a time. *Science* 2006 MAR 17;311(5767):1600-3.

Zdrojewicz Z, Pachura E, Pachura P. The Thymus: A Forgotten, But Very Important Organ. *Adv.Clin.Exp.Med.* 2016 MAR-APR;25(2):369-75.

Zhou E, Lim C, Quek S. Finite element simulation of the micropipette aspiration of a living cell undergoing large viscoelastic deformation. *Mechanics of Advanced Materials and Structures* 2005 NOV-DEC;12(6):501-12.

Zhou ZL, Ngan AHW, Tang B, Wang AX. Reliable measurement of elastic modulus of cells by nanoindentation in an atomic force microscope. *Journal of the Mechanical Behavior of Biomedical Materials* 2012 APR 2012;8:134-42.

Zhu C, Bao G, Wang N. Cell mechanics: Mechanical response, cell adhesion, and molecular deformation. *Annu.Rev.Biomed.Eng.* 2000 2000;2:189-226.

## Supplementary information

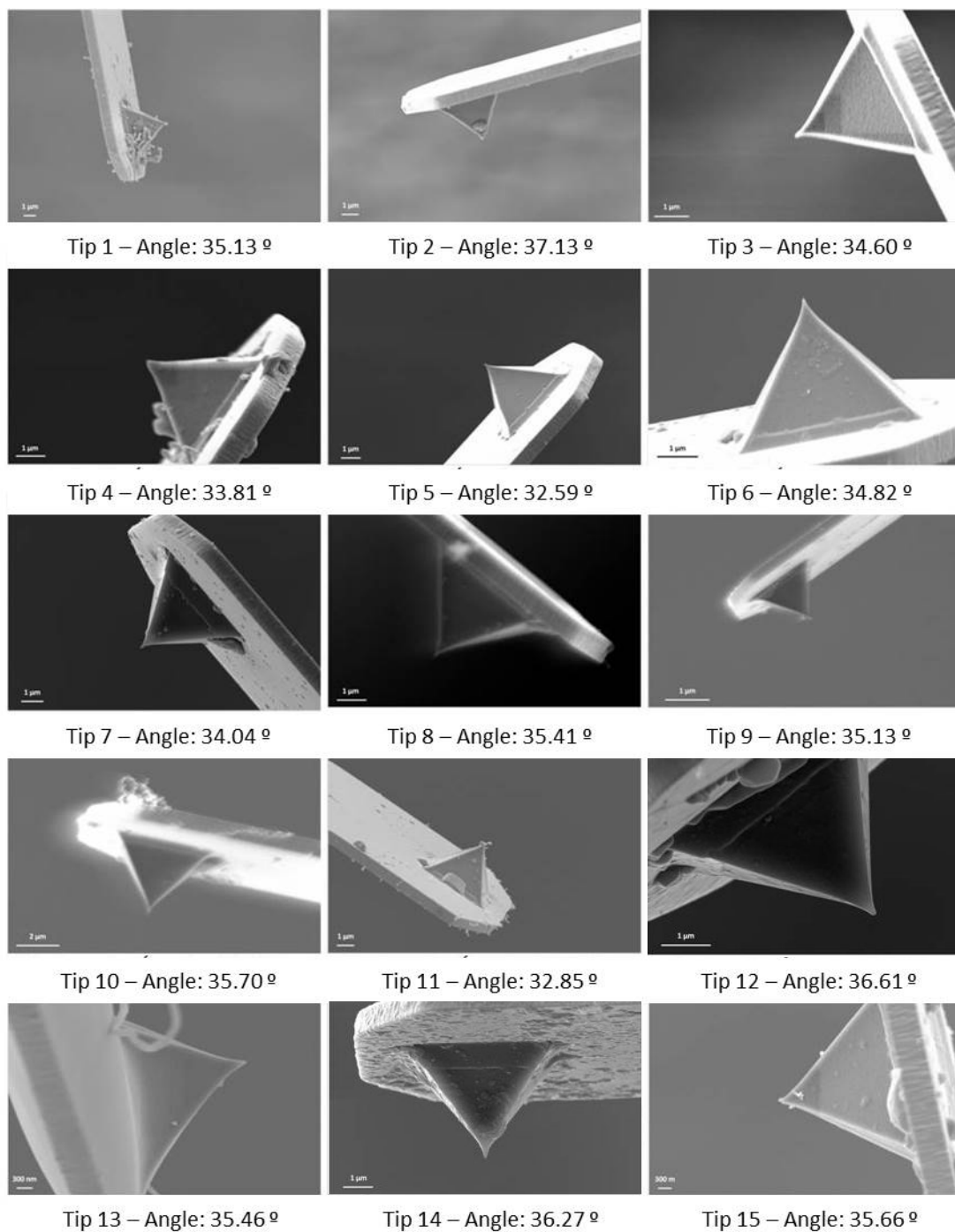


Figure S1. Some examples of AFM tip FSEM images.